

Ultra-low acoustic-phonon-limited mobility and giant phonon-drag thermopower in MgZnO/ZnO heterostructures

Margarita Tsaousidou^{*,1}

¹ Materials Science Department, University of Patras, Patras 26 504, Greece

Received XXXX, revised XXXX, accepted XXXX

Published online XXXX

Key words: MgZnO/ZnO heterostructures, electron-phonon coupling, acoustic-phonon-limited mobility, phonon-drag thermopower

* Corresponding author: e-mail rtsaous@upatras.gr

We present numerical simulations of the acoustic-phonon-limited mobility, μ_{ac} , and phonon-drag thermopower, S^g , in two-dimensional electron gases confined in MgZnO/ZnO heterostructures. The calculations are based on the Boltzmann equation and are made for temperatures in the range 0.3-20 K and sheet densities $0.5\text{-}30 \times 10^{15} \text{ m}^{-2}$. The theoretical estimations of μ_{ac} are in good agreement with the experiment without any adjustable parameters. We find that the magnitude of μ_{ac}

is dramatically decreased in relation to GaAs based heterostructures. The phonon-drag thermopower, S^g , which according to Herring's expression is inversely proportional to μ_{ac} is severely increased exceeding 200 mV/K at $T = 5$ K depending on sheet density. The giant values of S^g lead to a strong improvement of the figure of merit ZT at low temperatures. Our findings suggest that MgZnO/ZnO heterostructures can be candidates for good thermoelectric materials at cryogenic temperatures.

Copyright line will be provided by the publisher

1 Introduction In the last few years the transport properties of two-dimensional electron gases (2DEGs) confined in MgZnO/ZnO heterostructures have attracted a considerable amount of research interest. Recent advances on growth techniques have enabled the realization of very clean 2DEGs with mobilities reaching $8 \times 10^5 \text{ cm}^2/\text{Vs}$ [1, 2, 3] and the observation of the integer [4] and the fractional quantum Hall effect [1, 2, 3, 5]. In addition 2DEGs in MgZnO/ZnO heterostructures are ideal systems for studying correlation effects [6] because the interaction parameter $r_s = (\sqrt{\pi n_s} \alpha_B^*)^{-1}$ (with n_s being the sheet density and α_B^* the effective Bohr radius) is much larger compared to the one in AlGaAs/GaAs heterostructures mainly due to the larger effective mass in ZnO based materials.

In this Letter we study the effect of electron coupling with acoustic phonons on the mobility and thermopower. So far theoretical studies have been successful in interpreting mobility data at low T by introducing charged-impurity and interface-roughness scattering [7] but the higher T -regime where acoustic phonons become important has re-

mained unexplored until now. Recently Falson *et al* [2] presented a set of mobility data in MgZnO/ZnO heterostructures in the temperature range 0.3-20 K and for sheet densities 0.7 to $20 \times 10^{15} \text{ m}^{-2}$. These data show clear evidence of acoustic-phonon scattering at higher T . Here we present numerical simulations of the acoustic-phonon-limited mobility, μ_{ac} , that are based on the semiclassical Boltzmann equation [8] and we obtain good agreement with the mobility data of Ref. [2] without adjustable parameters. It is found that μ_{ac} in MgZnO/ZnO heterostructures is reduced by over two orders of magnitude in relation to GaAs based quantum wells (QWs).

We also investigate, for the first time, the phonon-drag thermopower, S^g , in 2DEGs confined in MgZnO/ZnO heterostructures. S^g is the contribution to thermopower that arises due to the momentum exchange between electrons and non-equilibrium acoustic phonons in the presence of a weak in-plane ∇T . Phonon-drag thermopower in 2DEGs has been extensively studied in both a theoretical and an experimental level [9, 10]. According to Herring's expres-

Copyright line will be provided by the publisher

sion [11] S^g is inversely proportional to μ_{ac} . Consequently in ZnO based 2D systems we expect a dramatic increase of S^g in relation to GaAs QWs. Namely, for the samples of Ref. [2] we find that the magnitude of S^g exceeds 200 mV/K depending on sheet density. These are the larger values that have been predicted so far for 2DEGs systems. Due to the huge magnitude of S^g a strong enhancement of ZT is predicted at low T .

2 Theory We assume that the 2DEG lies on the xy -plane. The acoustic-phonon-limited mobility that is related to the scattering of 2D electrons with wave vector $\mathbf{k} = (k_x, k_y)$ by 3D acoustic phonons with wave vector $\mathbf{Q} = (\mathbf{q}, q_z)$ is obtained from [8]

$$\mu_{ac}^{-1} = \frac{m^*}{e} \left\langle \frac{1}{\tau_{ac}} \right\rangle, \quad (1)$$

where m^* is the electron effective mass, e is the magnitude of the electron charge and $\langle 1/\tau_{ac} \rangle$ is a suitable average over the electron energy $\epsilon_{\mathbf{k}}$ of the microscopic electron-phonon (e-ph) scattering rate $1/\tau_{ac}$ given by [8]

$$\left\langle \frac{1}{\tau_{ac}} \right\rangle = \frac{\int d\epsilon_{\mathbf{k}} \epsilon_{\mathbf{k}} [df^0(\epsilon_{\mathbf{k}})/d\epsilon_{\mathbf{k}}] \langle 1/\tau_{ac}(\epsilon_{\mathbf{k}}) \rangle}{\int d\epsilon_{\mathbf{k}} \epsilon_{\mathbf{k}} [df^0(\epsilon_{\mathbf{k}})/d\epsilon_{\mathbf{k}}]}, \quad (2)$$

where $f^0(\epsilon_{\mathbf{k}})$ is the Fermi-Dirac function. $1/\tau_{ac}$ is obtained by solving the Boltzmann equation in the presence of a weak electric field in the relaxation time approximation. Then for the average $\langle 1/\tau_{ac} \rangle$ we get [8]

$$\left\langle \frac{1}{\tau_{ac}} \right\rangle = \frac{(2m^*)^{1/2}}{2\pi n_s \hbar^2 k_B T} \sum_{\lambda, \mathbf{Q}} q \frac{|U_{\mathbf{Q}\lambda}|^2}{\epsilon^2(q, T)} N_{\mathbf{Q}\lambda}^0 Z(q_z) \times \int_{\gamma}^{\infty} d\epsilon_{\mathbf{k}} \frac{f^0(\epsilon_{\mathbf{k}}) [1 - f^0(\epsilon_{\mathbf{k}} + \hbar\omega_{\mathbf{Q}\lambda})]}{\sqrt{\epsilon_{\mathbf{k}} - \gamma}}, \quad (3)$$

where λ denotes the phonon mode (one longitudinal and two transverse), $|U_{\mathbf{Q}\lambda}|^2$ is the square of the e-ph coupling matrix elements, $\epsilon(q, T)$ is the static 2D dielectric function, $\hbar\omega_{\mathbf{Q}\lambda}$ is the phonon energy, $N_{\mathbf{Q}\lambda}^0$ is the phonon distribution in equilibrium, $\gamma = (\hbar\omega_{\mathbf{Q}\lambda} - \epsilon_q)^2/4\epsilon_q$ (where $\epsilon_q = \hbar^2 q^2/2m^*$). Finally, $Z(q_z)$ is the form factor

$$Z(q_z) = \left| \int \phi_0^*(z) \exp(iq_z z) \phi_0(z) dz \right|^2 \quad (4)$$

where for the envelope function in the ground state $\phi_0(z)$ we use the Fang-Howard [12] wave functions.

The square of the e-ph matrix elements $|U_{\mathbf{Q}\lambda}|^2$ is

$$|U_{\mathbf{Q}\lambda}|^2 = \frac{\hbar Q^2 \Xi_{Eff}^2(\mathbf{Q}\lambda)}{2\rho V \omega_{\mathbf{Q}\lambda}} \quad (5)$$

where ρ and V are, respectively, the density and the volume of the sample. The term $\Xi_{Eff}(\mathbf{Q}\lambda)$ denotes the 'effective' acoustic potential describing the e-ph coupling and

accounts for both the deformation potential and the piezoelectric coupling. In ZnO the conduction band is isotropic and only longitudinal acoustic phonons are coupled with electrons via deformation potential coupling. In this case the deformation potential is described by a single constant Ξ_d . In semiconductors with wurtzite structure, such as ZnO, the contribution to $\Xi_{Eff}^2(\mathbf{Q}\lambda)$ due to piezoelectric e-ph coupling is [13]

$$\Xi_{Piez}^2(\mathbf{Q}\lambda) = \frac{e^2}{Q^6} \{ h_{15}(q_x^2 + q_y^2)(\mathbf{e}_{\mathbf{Q}\lambda})_z + h_{33}q_z^2(\mathbf{e}_{\mathbf{Q}\lambda})_z + (h_{15} + h_{31})q_z[q_x(\mathbf{e}_{\mathbf{Q}\lambda})_x + q_y(\mathbf{e}_{\mathbf{Q}\lambda})_y] \}^2, \quad (6)$$

where $(\mathbf{e}_{\mathbf{Q}\lambda})_i$ is the i -component of the phonon polarization vector and h_{15} , h_{33} , h_{31} are the non-zero elements of the piezoelectric tensor.

The 2D dielectric function $\epsilon(q, T)$ has the form [14, 15]

$$\epsilon(q, T) = 1 + \frac{e^2}{2\epsilon_0 \epsilon_r q} \Pi(q, T) F(q) \xi(q) [1 - G(q)], \quad (7)$$

where ϵ_0 is the permittivity of vacuum, ϵ_r is the relative permittivity of ZnO, $\Pi(q, T)$ is the polarisability [16], $F(q)$ is the screening form factor that accounts for the finite extent of the electron wave function in the z -direction [15], $\xi(q) = 1$ when $q/2k_F < 1$ and $\xi(q) = 1 - \sqrt{1 - (2k_F/q)^2}$ when $q/2k_F \geq 1$ (with k_F being the Fermi wave number). $G(q)$ is the local-field correction (LFC) factor that describes exchange and correlation effects beyond the random-phase approximation. It is given by [14]

$$G(x) = r_s^{2/3} \frac{1.402x}{\sqrt{2.644C_{12}^2 + x^2 C_{22}^2}}, \quad (8)$$

where $x = q/q_0$ and $q_0 = 2/(\tau_s^{2/3} \alpha_B^*)$. C_{12} and C_{22} depend on r_s and their expressions are given in Ref. [14]. We note that the LFC becomes important at low densities where the interaction parameter r_s becomes large.

The phonon-drag thermopower is related to μ_{ac} via Herring's expression [11]. Although Herring's expression was phenomenological when it was first proposed, later studies [8, 17] based on the semiclassical Boltzmann framework showed that this expression was precise in 2DEGs. We can write [8, 17]

$$S^g = - \sum_{\lambda} \frac{v_s^{\lambda} l_{ph} m^*}{eT} \left\langle \frac{1}{\tau_{ac}^{\lambda}} \right\rangle = - \sum_{\lambda} \frac{v_s^{\lambda} l_{ph}}{T} \left\langle \frac{1}{\mu_{ac}^{\lambda}} \right\rangle, \quad (9)$$

where v_s^{λ} is the sound velocity for the λ mode and l_{ph} is the phonon-mean-free path which is assumed to be λ -independent. At low temperatures l_{ph} is determined by boundary phonon scattering and depends only on the dimensions of the sample. Detailed numerical calculations showed that the average $\langle 1/\mu_{ac} \rangle$ describes accurately the inverse of acoustic-phonon-limited mobility.

3 Numerical simulations and comparison with the experiment The values for the parameters used in the calculations are $m^* = 0.29 m_e$ (see, for example, Ref. [7]), $v_s^L = 6167$ m/s and $v_s^T = 2561$ m/s [18], $\epsilon_r = 8.5$ [7], $\rho = 6.1 \times 10^3$ Kg/m³ [19], and $\Xi_d = 15$ eV [19], $h_{15} = -6.4 \times 10^9$ V/m, $h_{31} = -7.6 \times 10^9$ V/m, and $h_{33} = 17.5 \times 10^9$ V/m [20].

In Fig.1 the dots are the experimental data [2] for the total mobility in four samples with sheet densities $1.4, 1.7, 4.5$ and 7×10^{15} m⁻². The red dashed lines are the numerical simulations of μ_{ac} based on Eqs. (1)-(8). The total mobility is obtained by $\mu_{tot}^{-1} = \mu_{ac}^{-1} + \mu_{el}^{-1}$ where μ_{el} is the mobility limited by elastic scattering (μ_{el} is obtained from the data at $T = 0.3$ K). The calculations of μ_{tot} are shown as blue solid lines. The agreement with the experiment is good without adjustable parameters. Good agreement was found also for another sample with $n_s = 20 \times 10^{15}$ m⁻² while for a very dilute sample with $n_s = 0.68 \times 10^{15}$ m⁻² the theory underestimates the data by a factor of two at the highest T examined (not shown here).

The effect of the LFC term $G(q)$ in the dielectric function is shown in Fig.2 for a dilute sample with $n_s = 1.4 \times 10^{15}$ m⁻² ($r_s = 9.7$). The calculations of μ_{ac} without the incorporation of the $G(q)$ term in Eq. (7) are enhanced by over a factor of three (green dashed-dotted line). In Fig.2 we show also the calculations of μ_{ac} for a 2DEG confined in an AlGaAs/GaAs heterostructure (black dotted line) with the same sheet density. We see that μ_{ac} in MgZnO/ZnO heterostructures is severely suppressed in relation to GaAs/AlGaAs counterparts.

The dependence of μ_{ac} on sheet density is shown in Fig.3. Inspection of Eq.(3) shows that at low T ($q \ll 2k_F$) and for degenerate 2DEGs μ_{ac} varies as $n_s^{3/2}$. The deviation observed at low n_s is due to the breakdown of the

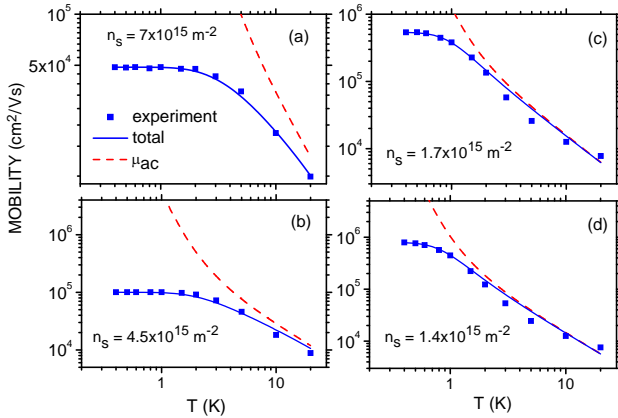


Figure 1 Mobility as a function of temperature for four samples with sheet densities $1.4, 1.7, 4.5,$ and 7×10^{15} m⁻². The blue solid and the red dashed lines denote the calculations of the μ_{tot} and μ_{ac} , respectively. The symbols are the experimental data [2].

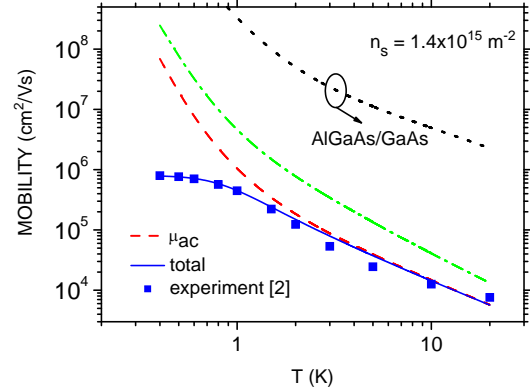


Figure 2 Mobility as a function of temperature for the sample with $n_s = 1.4 \times 10^{15}$ m⁻². The green dashed-dotted line shows the results for μ_{ac} when the local-field correction is ignored. The calculation of μ_{ac} for an AlGaAs/GaAs heterostructure with the same n_s is shown as black dotted line.

low- T approximations. The elastic scattering is strong at low temperatures for the samples with densities higher than 1.7×10^{15} m⁻² and we cannot identify μ_{ac} accurately. For this reason we do not present the relevant data in Fig.3a.

In Fig.4a we show the calculations of $-S^g$ by using Eqs.(3)-(9) for three 2DEGs confined in MgZnO/ZnO het-

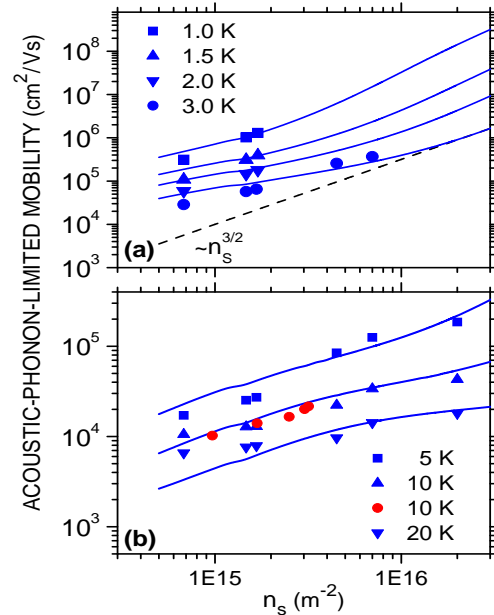


Figure 3 Acoustic-phonon-limited mobility as a function of sheet density for T in the range 1-20 K. The solid lines are the numerical simulations and the symbols are the experimental data from Ref.[2] (blue) and Ref.[1] (red).

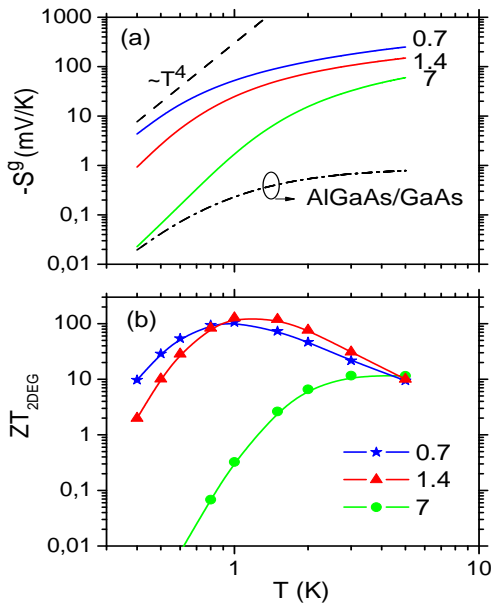


Figure 4 $-S^g$ (a) and ZT_{2DEG} (b) as a function of T for three 2DEGs in a MgZnO/ZnO heterointerface with $n_s = 0.7, 1.4$ and $7 \times 10^{15} \text{ m}^{-2}$. In (a) the dashed-dotted line refers to a 2DEG in an AlGaAs/GaAs heterostructure with $n_s = 0.7 \times 10^{15} \text{ m}^{-2}$.

erostructures with sheet densities 0.7 (blue line), 1.4 (red line) and $7 \times 10^{15} \text{ m}^{-2}$ (green line). l_{ph} is taken to be 1 mm. At low T S^g follows a T^4 law which is characteristic for piezoelectric e-ph coupling [10]. In the same figure we present also the calculations of $-S^g$ for a 2DEG in an AlGaAs/GaAs heterostructure with $n_s = 0.7 \times 10^{15} \text{ m}^{-2}$. Quite remarkably the magnitude of phonon drag is dramatically enhanced in MgZnO/ZnO heterostructures exceeding 200 mV/K at $T = 5$ K for low n_s . This huge increase is due to the following characteristics of ZnO based 2D structures: (i) the large effective mass, (ii) the strong piezoelectric e-ph coupling, and (iii) the decrease of the screening effects due to exchange and correlation effects. (The same characteristics are responsible for the ultra-low μ_{ac} .)

We note that at low T the diffusion thermopower overwhelms S^g . For the 2DEGs in a MgZnO/ZnO heterostructure shown in Fig. 4 the crossover occurs at T in the range 0.1-0.2 K assuming small-angle electron scattering.

The giant $-S^g$ results to a significant enhancement of the thermoelectric efficiency at low T . The calculations of the figure of merit ZT_{2DEG} for the 2DEGs confined in MgZnO/ZnO heterostructures with $n_s = 0.7, 1.4$, and $7 \times 10^{15} \text{ m}^{-2}$ are shown in Fig.4b. More analytically for ZT_{2DEG} we use the expression $ZT_{2DEG} = (S^g)^2 \sigma T / \kappa_{ph}$ where $\sigma = n_s e \mu_{tot} / w$ with w being the thickness of the 2DEG (we assume that $w = 10$ nm) and $\kappa_{ph} = 4860 l_{ph} T^3$ is the phonon conductivity in the Debye approximation. We note that ZT_{2DEG} is proportional to l_{ph} .

At low T l_{ph} is specified by the dimensions of the sample and can be a few mm. Thus ZT_{2DEG} can be even larger than what shown in Fig.4b where l_{ph} is taken to be 1 mm. In the calculation of the figure of merit we use the thickness of a single layer. The conductivity of the barrier layer is smaller than that of the 2DEG layer. The effective conductivity is $\sigma_{eff} = \sigma / (1 + N_{barrier})$ [21] where $N_{barrier}$ is the number of the unit cells of the barrier layer. Consequently, ZT_{2DEG} is decreased by the factor $1 + N_{barrier}$.

4 Conclusions In summary, we predict an ultra-low acoustic-phonon-limited mobility and a giant phonon-drag thermopower in MgZnO/ZnO heterostructures. The theoretical estimates of μ_{ac} are in very good agreement with the experiment without adjustable parameters. This gives us confidence about our understanding of the mechanisms of e-ph coupling in the present system and the accuracy of our calculations for S^g . We find that at low T the magnitude of S^g can exceed 200 mV/K. This value of S^g is the largest ever predicted in 2DEGs. Finally, we predict a dramatic increase of the effective figure of merit that depends on the sheet density, the phonon-mean-free path and the number of barrier layers.

Acknowledgements The author wishes to thank Dr. Falson for providing the mobility data of Ref.[2] appearing in Fig.1, Fig.2, and Fig.3.

References

- [1] A. Tsukazaki *et al.*, Nature Mater. **9**, 889 (2010).
- [2] J. Falson *et al.*, Appl. Phys. Express **4**, 091101 (2011).
- [3] D. Maryenko *et al.*, Phys. Rev. Lett. **108**, 186803 (2012).
- [4] A. Tsukazaki *et al.*, Science **315**, 1388 (2007).
- [5] Y. Kozuka *et al.*, Phys. Rev. B **85**, 075302 (2012).
- [6] Y. Kasahara *et al.*, Phys. Rev. Lett. **109**, 246401 (2012).
- [7] A. Gold, Appl. Phys. Lett. **96**, 242111 (2010); A. Gold, J. Appl. Phys. **110**, 043702 (2011).
- [8] M. Tsaousidou *et al.*, Phys. Rev. B **64**, 165304 (2001).
- [9] B. L. Gallagher and P. N. Butcher, in Handbook on Semiconductors, edited by P. T. Landsberg (Elsevier, Amsterdam, 1992), vol. 1, p. 817; R. Fletcher, E. Zaremba, and U. Zeitler, in Electron-Phonon Interactions in Low-Dimensional Structures, edited by L. Challis (Oxford Science Publications, Oxford, 2003), p. 149.
- [10] M. Tsaousidou, in The Oxford Handbook of Nanoscience and Technology, edited by A. V. Narlikar and Y. Y. Fu (Oxford University Press, Oxford, 2010), vol. II, p. 477.
- [11] C. Herring, Phys. Rev. **96**, 1163 (1954).
- [12] F. F. Fang and W. E. Howard, Phys. Rev. Lett. **16**, 797 (1966).
- [13] B. Krummheuer *et al.*, Phys. Rev. B **71**, 235329 (2005).
- [14] A. Gold and L. Calmels, Phys. Rev. B **48**, 11622 (1993).
- [15] T. Ando *et al.*, Rev. Mod. Phys. **54**, 437 (1982).
- [16] P. F. Maldague, Surf. Sci. **73**, 296 (1978).
- [17] A. Miele *et al.*, Phys. Rev. B **58**, 13181 (1998).
- [18] K. Sarasamak *et al.*, Phys. Rev. B **82**, 035201 (2010).
- [19] D. C. Look, Sem. Sci. Tech. **20**, S55 (2005).

- [20] B. A. Auld, in *Acoustic Fields and Waves in Solids*, (John Wiley and Sons, USA, 1973), vol. I, p. 378.
- [21] H. Ohta *et al.*, *Nature Mater.* **6**, 129 (2007).